Hindawi
International Journal of Aerospace Engineering
Volume 2020, Article ID 1916239, 16 pages
https://doi.org/10.1155/2020/1916239

Research Article

Aeroacoustic Attenuation Performance of a Helmholtz Resonator with a Rigid Baffle Implemented in the Presence of a Grazing Flow

Di Guan,[1] **Dan Zhao**,[1] **and Zhaoxin Ren**[2]

[1]*Department of Mechanical Engineering, College of Engineering, University of Canterbury, Private Bag 4800, Christchurch 8140, New Zealand*
[2]*School of Power and Energy Engineering, Northwestern Polytechnical University, Xi'an 710072, China*

Correspondence should be addressed to Dan Zhao; dan.zhao@canterbury.ac.nz

Received 1 April 2019; Revised 22 July 2019; Accepted 9 December 2019; Published 19 April 2020

Academic Editor: Enrico Cestino

Copyright © 2020 Di Guan et al. This is an open access article distributed under the Creative Commons Attribution License, which permits unrestricted use, distribution, and reproduction in any medium, provided the original work is properly cited.

To broaden its' effective frequency range and to improve its transmission loss performance, a modified design of a Helmholtz resonator is proposed and evaluated by implementing a rigid baffle in its cavity. Comparison is then made between the proposed design and the conventional one by considering a rectangular duct with the resonator implemented in the presence of a mean grazing flow. For this, a linearized 2D Navier-Stokes model in frequency domain is developed. After validated by benchmarking with the available experimental data and our experimental measurements, the model is used to evaluate the effects of (1) the width L_p of the rigid baffle, (2) its implementation location/height H_g, (3) its implementation configurations (i.e., attached to the left sidewall or right sidewall), (4) the grazing mean flow M_u (Mach number), and (5) the neck shape on a noise damping effect. It is shown that as the rigid baffle is attached in the 2 different configurations, the resonant frequencies and the maximum transmission losses cannot be predicted by using the classical theoretical formulation $\omega^2 = c^2 S/VL_{eff}$, especially as the grazing Mach number M_u is greater than 0.07, i.e., $M_u > 0.07$. In addition, there is an optimum grazing flow Mach number corresponding to the maximum transmission loss peak, as the width L_p is less than half of the cavity width D_r, i.e., $L_p/D_r \leq 0.5$. As the rigid plate width is increased to $L_p/D_r = 0.75$, one additional transmission loss peak at approximately 400 Hz is produced. The generation of the 12 dB transmission loss peak at 400 Hz is shown to attribute to the sound and structure interaction. Finally, varying the neck shape from the conventional one to an arc one leads to the dominant resonant frequency being increased by approximately 20% and so the secondary transmission loss peak by 2-5 dB. The present work proposes and systematically studies an improved design of a Helmholtz resonator with an additional transmission loss peak at a high frequency, besides the dominant peak at a low frequency.

1. Introduction

Helmholtz resonators are widely applied in automobile [1] and aerospace industries as an effective acoustics noise damper [2, 3]. Compared with other dampers, such as half- and quarter-wave resonators, Helmholtz resonators are found to be associated with a higher noise damping capacity [4]. They are typically coupled to an engine in the presence of a mean flow, which is also known as a grazing flow. To achieve its maximum noise attenuation performance, these resonators need to be well-designed so that they are tuned to the natural resonant frequencies [5]. Poor noise damping performances are generally expected, when the noise frequency is quite different from the near-resonant one, i.e., off-resonance conditions. The resonant frequencies can be predicted by using $\omega^2 = c^2 S/VL_{eff}$. Here, c denotes the speed of sound. V is the resonator cavity volume. L_{eff} and S denote the effective length and the cross-sectional

area of the resonator neck. L_{eff} is greater than the neck physical length due to the end correction effect [6, 7]. Chanaud [6] developed a theoretical equation to determine the end correction.

The classical theoretical formula $\omega^2 = c^2 S/VL_{\text{eff}}$ to predict the resonant frequency [8] fails in capturing the geometry shape of the resonator cavity and its neck, since it is derived by using a lumped mass model. Neither is the mean flow effect considered. The neck asymmetry is found to affect the resonant frequencies for both rectangular and cylindrical resonators [9]. Mercier et al. [10] confirmed the critical role of the neck shape on affecting noise damping capacity of Helmholtz resonators by conducting theoretical analysis via homogenization means. The noise damping mechanism is mainly due to a thermoviscous effect [11] and/or vortex shedding. Nonlinear damping [12] could be involved, depending on the amplitude of the incident sound to the resonator. To achieve optimum noise damping, acoustic resonance is expected, at which a large volume of the working fluid in the cavity periodically expands and compresses. This means that if the resonator cavity is structurally modified, the resonant frequency and the effective bandwidth are then varied. This is confirmed by extending the neck into the cavity [13] or filling porous materials in the resonator cavity [14]. However, alternative structural modification is expected. This partially motivated the present work.

Two or more Helmholtz resonators could be applied to broaden the effective frequency range in practice. Tang and Sirignano [15] derive a generalized theoretical model to predict a conventional Helmholtz resonator's damping performance. It is found that long damping resonator should not be applied in practical designs. Li and Cheng [16] develop a generalized model to study the acoustic response of a Helmholtz resonator array coupled with an enclosure. A frequency formula is derived, which can be used to determine the variation at off-designed and designed conditions. Griffin et al. [17] experimentally study the noise attenuation performance of mechanically coupled Helmholtz resonators. It is found that a wider bandwidth is achievable. Similar coupled Helmholtz resonators are theoretically and experimentally studied by Johansson and Kleiner [18]. Xu et al. [19] propose and test two coupled Helmholtz resonators in the configuration of neck-cavity-neck-cavity. It is found that the geometric shape of the 2nd cavity affects little on the resonant frequencies. However, increasing the length of the 2nd resonator neck leads to the resonant frequencies being decreased. Similar configuration of coupled Helmholtz resonators is proposed by Cai and Mak [20]. A broader bandwidth is achieved. Slaton and Nishikawa [21] propose to mount two Helmholtz resonators coaxially on a cylindrical due in a presence of a low Mach number mean flow. It is found that 90-degree bending of the resonator necks has a little effect on changing the aeroacoustic damping response of the resonator network.

The aeroacoustic damping performance of a conventional Helmholtz resonator may be improved by implementing a vibrating sidewall or back-wall of its cavity. Nudehi et al. [22] design and test a Helmholtz resonator with a flexible backplate. Multiple resonant peaks are found in comparison with a single peak of the conventional resonator with a rigid backplate. The idea of applying a flexible plate is adopted by Zhao [23] to study the transmission loss performance of a parallel-coupled Helmholtz resonator network. Further applying tunable backplate is evaluated by Zhang et al. [24] to minimize combustion-driven periodic noises in a Rijke tube combustor. 50 dB sound pressure level is achieved. The tunable resonator works well even at off-design conditions [23, 24]. In industrial engine applications, the mean grazing flow is hot. It affects the acoustic damping performances of Helmholtz resonators. Ćosić et al. [25] experimentally study the acoustic noise damping performance of Helmholtz resonators, when the grazing and cooling flows have a temperature difference between them. The temperature difference is found to affect strongly on the resonant frequency of the resonator and its noise damping performance.

Extensive theoretical, experimental [26, 27], and numerical studies [28] are conducted on the noise attenuating performances of Helmholtz resonators in different geometric shapes or by introducing additional components [13, 14, 26–28]. Yang et al. [29] conducted experimental measurements of the acoustic impedance of a Helmholtz resonator. Its neck is filled with perforated ceramics. A higher power absorption coefficient and a broader effective frequency range are found. In general, foregoing studies are conducted to improve the acoustic noise damping performance and/or broaden the effective frequency ranges of Helmholtz resonators. Extensive researches are ongoing to achieve an optimum or a better design of a Helmholtz resonator. This motivated partially the current study.

In this work, a rectangular Helmholtz resonator with a rigid baffle attached inside its cavity is proposed and systematically studied. The resonator is flushed mounted on a rectangular duct with a mean grazing flow. For this, 2D numerical investigations are performed in frequency domain via determining the solutions of linearized NS (Navier-Stokes) equations. This is done by using COMSOL 5.4. In Section 2.1, the system equations and the 2D model are described. The dominant variables are evaluated. These parameters include (1) the geometric width L_{p} of the rigid baffle, (2) its relative height/location H_{g} attached in the cavity, (3) the implementation configuration of the rigid baffle (i.e., attached to the left or the right sidewall), (4) the grazing flow Mach number M_{u}, and (5) the neck shape. In Section 2.2, the numerical 2D model is validated first. This is achieved by benchmarking with available experimental data. In Section 3, the 2D model is then modified and used to study the acoustic attenuating performances of the designed Helmholtz resonator. These impacts of the identified 5 design parameters are compared and discussed. Key findings are summarized in Section 4.

2. Description of the Model and Validation Studies

2.1. Description of the System Equations. In the present work, a 2D rectangular pipe with a rectangular Helmholtz resonator (HR) implemented is considered. It is illustrated

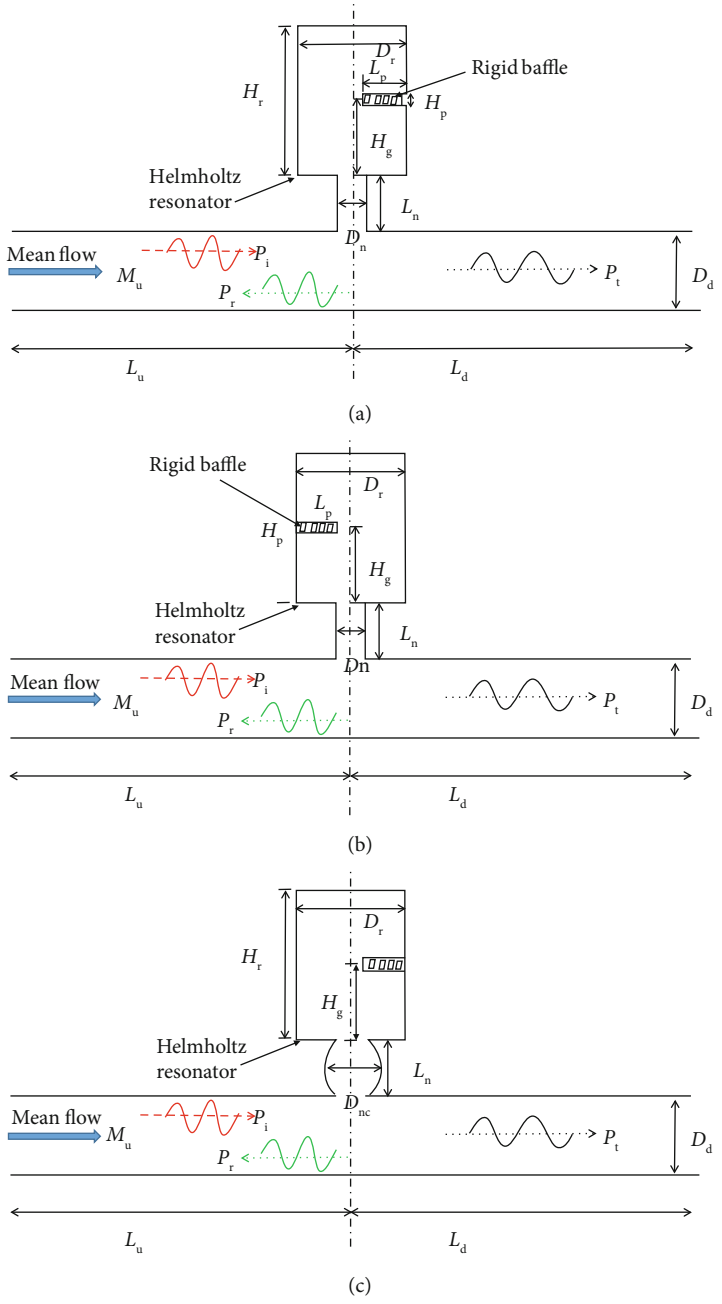

FIGURE 1: Schematics of a rectangular duct with a modified structured HR (Helmholtz resonator) implemented in the presence of a mean flow (i.e., grazing flow). Here, a rigid baffle is implemented in the resonator's cavity to change its aeroacoustic damping performances. (a) configuration 1 of the modified resonator, (b) configuration 2 of the modified resonator, and (c) the modified resonator with an arc-shaped neck.

schematically in Figure 1. The HR is axially implemented at $x = L_u$. There is a mean duct flow [28] with a Mach number of M_u. It is also known as the grazing flow. The air flow is assumed to be compressible and viscous. Thus, the NS equations could be linearized and be the governing one in frequency domain. The dimensions of the modelled rectangular pipe with a HR [1] used are summarized in Table 1. The physical dimensions and geometric shape are exactly the same as the experimental one in Ref. [1].

The system equations consist of the mass, momentum, and energy conservation ones [1, 8]. The working air is assumed to behave like a perfect gas. Molecular diffusion of heat and gravity forces are neglected (i.e., $\lambda = 0$ and $g_i = 0$). These governing equations are then given in time domain as

$$\frac{\partial \rho}{\partial t} + \frac{\partial}{\partial x_i}(\rho u_i) = 0, \tag{1}$$

$$\frac{\partial}{\partial t}(\rho u_i) + \frac{\partial}{\partial x_j}(\rho u_i u_j) + \frac{\partial p}{\partial x_i} = \frac{\partial \tau_{ij}(u_k)}{\partial x_j}, \tag{2}$$

$$\frac{\partial p}{\partial t} + u_i \frac{\partial p}{\partial x_i} + c^2 \rho \frac{\partial u_i}{\partial x_i} = (\kappa - 1)\tau_{ij}(u_k)\frac{\partial u_i}{\partial x_j}, \quad (3)$$

where the viscous stress is defined as $\tau_{ij}(u_k) = \mu((\partial u_i/\partial x_j) + (\partial u_j/\partial x_i) - (2/3)(\partial u_k/\partial x_k)\delta_{ij})$. ρ, u_i, and p denote the instantaneous density, velocity vector, and pressure variables; c denotes the speed of sound. κ is the ratio of specific heats of the air.

The thermodynamic state equation also holds as $p = \rho RT$. The compressible Navier-Stokes equations, i.e., Equations (1)–(3), can be linearized to obtain the acoustic governing equations. The instantaneous variables are assumed to consist of a mean and a fluctuating part. In physics, it means that a small-amplitude fluctuation (denoted by a prime) is superimposed on a mean flow filed (denoted by an overbar). In mathematics, it means that

$$\rho = \bar{\rho} + \rho', u_i = \bar{u}_i + u_i', p = \bar{p} + p'. \quad (4)$$

The fluctuating part of the air density, flow velocity, and pressure can be expressed in terms of Fourier series expansion as

$$\rho' = \hat{\rho}(\omega)e^{i\omega t}, \quad u_i' = \hat{u}_i(\omega)e^{i\omega t}, \quad p' = \hat{p}(\omega)e^{i\omega t}. \quad (5)$$

These quantities $\rho'/\bar{\rho}$, $|u_i'|/\bar{c}$, $p'/\bar{p}$, and $T'/\bar{T}$ are assumed to be a small order ε, where $\varepsilon < 1$ and $\bar{c}^2 = \kappa R\bar{T}$ is the mean speed of sound. Note that the mean part of the flow variables satisfies continuity of mass, momentum, and energy. An overhat in Equation (5) denotes the flow parameter in frequency domain.

Substituting Equation (4) into Equations (1)–(3) gives

$$\frac{\partial \rho'}{\partial t} + \frac{\partial}{\partial x_i}\left(\bar{u}_i\rho' + \bar{\rho}u_i'\right) = 0, \quad (6)$$

$$\frac{\partial \bar{\rho}u_i'}{\partial t} + \frac{\partial}{\partial x_j}\left(\overline{\rho u}_j u_i'\right) + \left(\bar{\rho}u_j' + \bar{u}_j\rho'\right)\frac{\partial \bar{u}_i}{\partial x_j} + \frac{\partial p'}{\partial x_i} = \frac{\partial \tau_{ij}\left(u_k'\right)}{\partial x_j}, \quad (7)$$

$$\frac{\partial p'}{\partial t} + \frac{\partial}{\partial x_i}\left(\bar{u}_i p' + \kappa\bar{p}u_i'\right) + (\kappa - 1)\left(p'\frac{\partial \bar{u}_i}{\partial x_i} + u_i'\frac{\partial \bar{p}}{\partial x_i}\right) = (\kappa - 1)\left[\left(\tau_{ij}(u_k)\frac{\partial u_i}{\partial x_j}\right)'\right]. \quad (8)$$

Equations (6)–(8) describe the spatiotemporal evolution of fluctuating quantities ρ', u_i', and p'. Note that the pressure fluctuation is selected as a primitive variable in the energy equation (Equation (8)). Furthermore, the source term of Equation (8) is attributed to the molecular stresses. The linearized mass conservation (Equation (6)) is needed to further simplify the linearized momentum (Equation (7)). By conducting linearization, any second-order terms are negligible. These include the term $u_i'u_j'$ characterizing the turbulence.

Table 1: Grazing flow, geometry, and physical sizes of the rectangular duct with the modified structured HR implemented.

Parameters	Values	Parameters	Values
L_u	0.65 cm	H_p	0.3 cm
L_d	65.0 cm	L_p/D_r	$0.25 \longrightarrow 0.75$
D_d	4.86 cm	$\overline{M_u}$	$0 \longrightarrow 0.1$
L_n	8.05 cm	$\bar{\rho}$	$1.2\,\mathrm{kg/m^3}$
D_n	0.0404 m	$\bar{p}$	101325 Pa
D_r	0.1532 m	$\omega/2\pi$	$50 \longrightarrow 500$Hz
H_r	24.42 cm	$\bar{T}$	297 K
H_g/H_r	$0.25 \longrightarrow 0.75$	D_{nc}	5.04 cm
Re ($M_u \geq 0.0029$)	≥3200		

Substituting Equation (5) into Equations (6)–(8) and eliminating the common factor of $e^{i\omega t}$ lead to the linearized Navier-Stokes equations in frequency domain as

$$i\omega\hat{\rho} + \frac{\partial}{\partial x_i}(\bar{u}_i\hat{\rho} + \bar{\rho}\hat{u}_i) = 0, \quad (9)$$

$$i\omega\bar{\rho}\hat{u}_i + \frac{\partial}{\partial x_j}\left(\overline{\rho u}_j\hat{u}_i\right) + \left(\bar{\rho}\hat{u}_j + \bar{u}_j\hat{\rho}\right)\frac{\partial \bar{u}_i}{\partial x_j} + \frac{\partial \hat{p}}{\partial x_i} = \frac{\partial \tau_{ij}(\hat{u}_k)}{\partial x_j}, \quad (10)$$

$$i\omega\hat{p} + \frac{\partial}{\partial x_i}(\bar{u}_i\hat{p} + \kappa\bar{p}\hat{u}_i) + (\kappa - 1)\left(\hat{p}\frac{\partial \bar{u}_i}{\partial x_i} + \hat{u}_i\frac{\partial \bar{p}}{\partial x_i}\right) = (\kappa - 1)\left[\left(\tau_{ij}(\hat{u}_k)\frac{\partial \hat{u}_i}{\partial x_j}\right)\right]. \quad (11)$$

These frequency domain governing Equations (9)–(11) are iteratively determined via COMSOL 5.4. Here, UMFPACK (a set of routines for solving unsymmetric sparse systems) direct solver and Menter's Shear Stress Transport (SST) turbulence model are applicable due to the nonnegligible duct/grazing flow, since it introduces much less numerical diffusion and leads to a better prediction of the eddy viscosity. The SST model is a combination of the k-ε model in the free stream and the k-ω model near the solid surface of the duct in order to capture the turbulence attenuation in details.

The unstructured meshes are illustrated in Figure 2. Mesh independence investigation is conducted first. In order to better capture the vortices and the shear layer at the duct-neck joint sections, a finer mesh with 1,260,360 cells is chosen. The selected mesh is enough by benchmarking the present predictions with the available (experimental) data in Refs. [26–28]. The benchmarking (i.e., validation) investigation is described in Section 2.2. The frequency step is set to 5 Hz and remains the same in all simulation cases. It will be confirmed that the frequency step is fine enough to produce good solutions. Note that the step could be decreased. However, a small frequency step gives rise to a significantly increased computational time

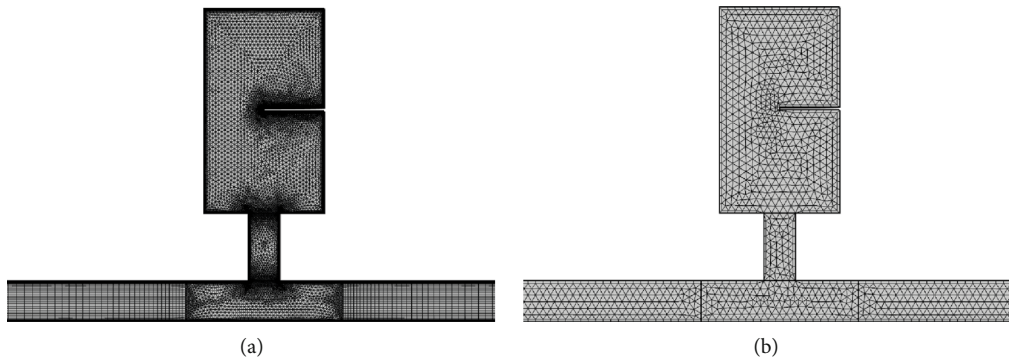

Figure 2: Computational unstructured mesh of the 2D-modelled duct with the modified Helmholtz resonator attached and a rigid baffle implemented: (a) 1,260,360 cells and (b) 63,920 cells.

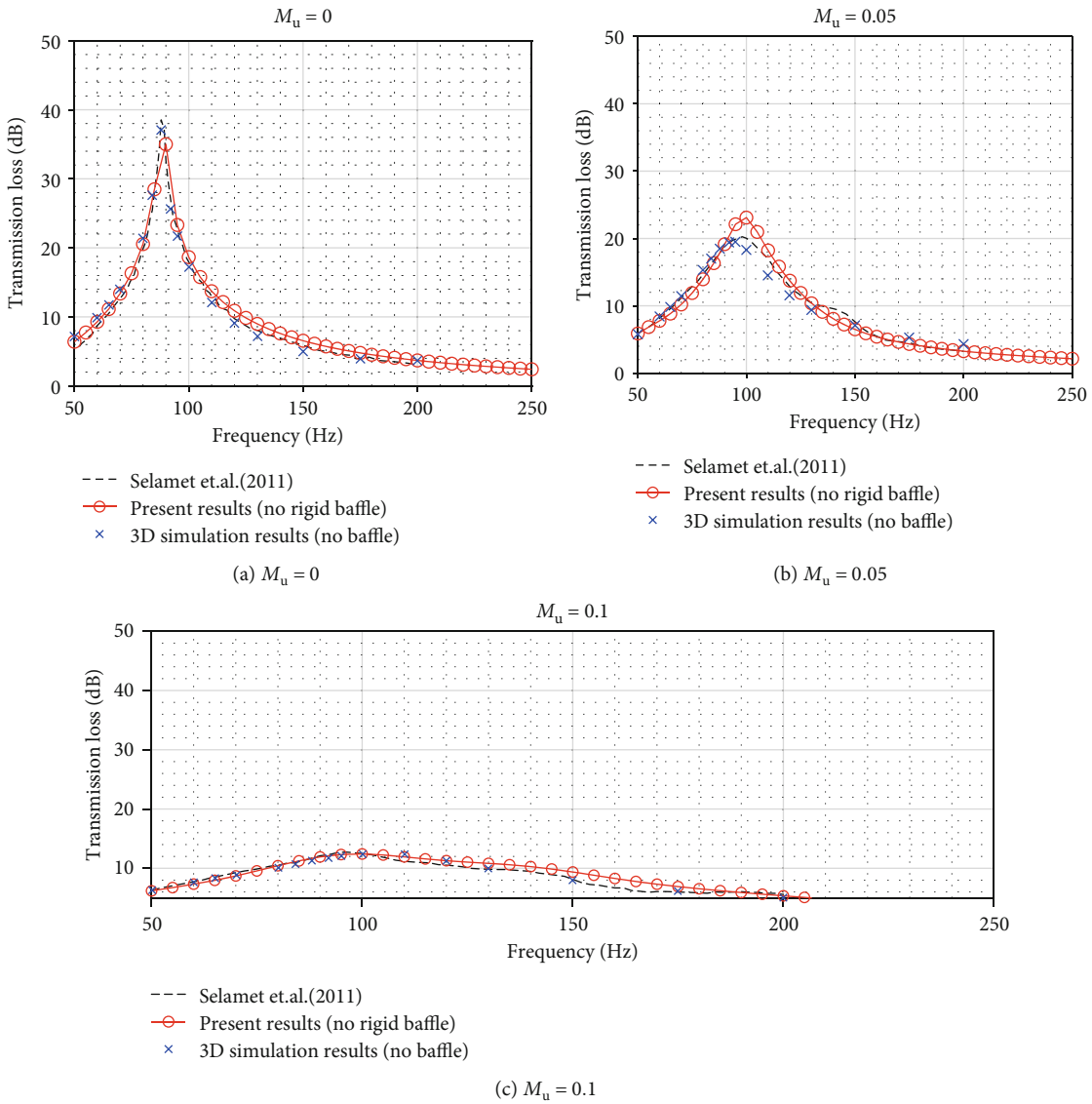

Figure 3: Comparing the current predicted transmission losses with those obtained from the present mode, 3D results [1] and the experimental ones Ref. [1].

and cost. Meanwhile, a smaller step is found to negligibly affect the transmission loss variation [21, 22]. Therefore, the frequency step is set to 5 Hz.

Plane travelling waves [23–26] are propagating along the duct and then passing through the HR. The boundary conditions of both duct ends are set to be PML (perfectly matched

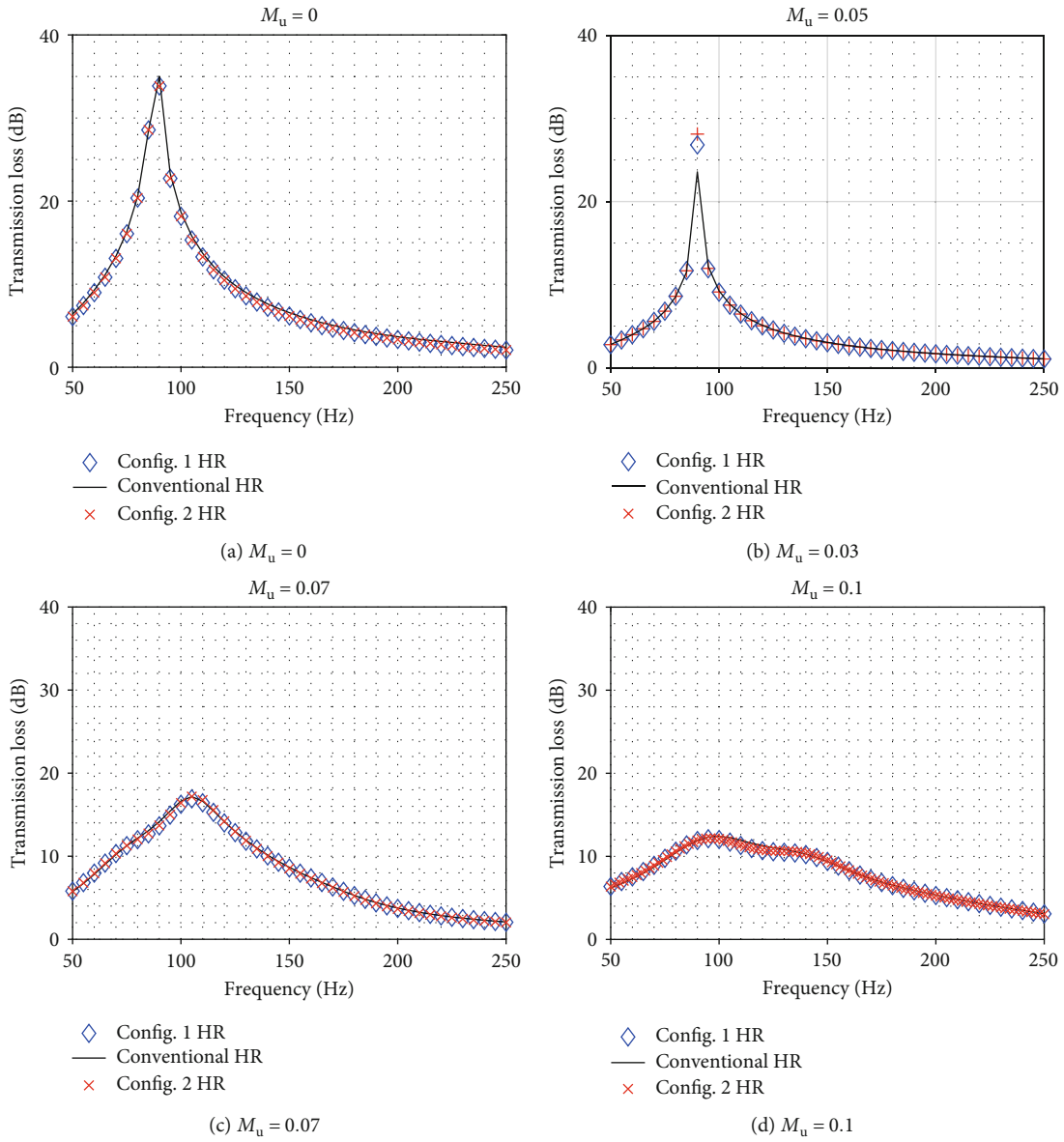

FIGURE 4: Comparison of transmission loss with a rigid baffle implemented in different configurations. Config. 1: $H_g/H_r = 0.5$, $L_p/D_r = 0.5$. Config. 2: $H_g/H_r = 0.5$, $L_p/D_r = 0.5$.

layer). To characterize the noise damping of the HR [30, 31], TL (transmission loss) is defined as

$$\mathrm{TL} \equiv 20 \log_{10}\left(\left\|\frac{\widehat{p}_i(\omega)}{\widehat{p}_t(\omega)}\right\|\right), \tag{12}$$

where p_i denotes the incident plane waves, and p_t is the transmitted wave in the upstream and downstream, respectively. It is worth noting that in practice, TL is experimentally determined via the classical TMT (two-microphone technique). It can be related to sound absorption coefficient, which is an alternative parameter widely used to indicate the noise damping performance of Helmholtz resonators [32, 33].

2.2. Validation Studies. In order to benchmark the developed model, comparison investigations are conducted on a 2D rectangular duct, as a grazing mean flow is present and a conventional Helmholtz resonator is implemented. Our numerical predictions are then compared with the experimental data available in Ref. [1] and 3D simulation results of the cylindrical duct and the cylindrical resonator. Note that all variables in the current numerical studies are chosen to be the same as the experimental investigations, for example, the geometry and physical dimensions of the HR and the duct, and the grazing flow conditions. To be consistent with the experimental measurements, the studied frequency range is set to be between 50 and 250 Hz. Figure 3 shows the comparison of transmission loss varied with acoustic frequency between the present numerical, 3D time-domain simulation (STAR-CD Ref. [1]) and experimental results, as the grazing flow Mach number M_u is set to 3 different values. It can be seen that for a given M_u, a good agreement between the

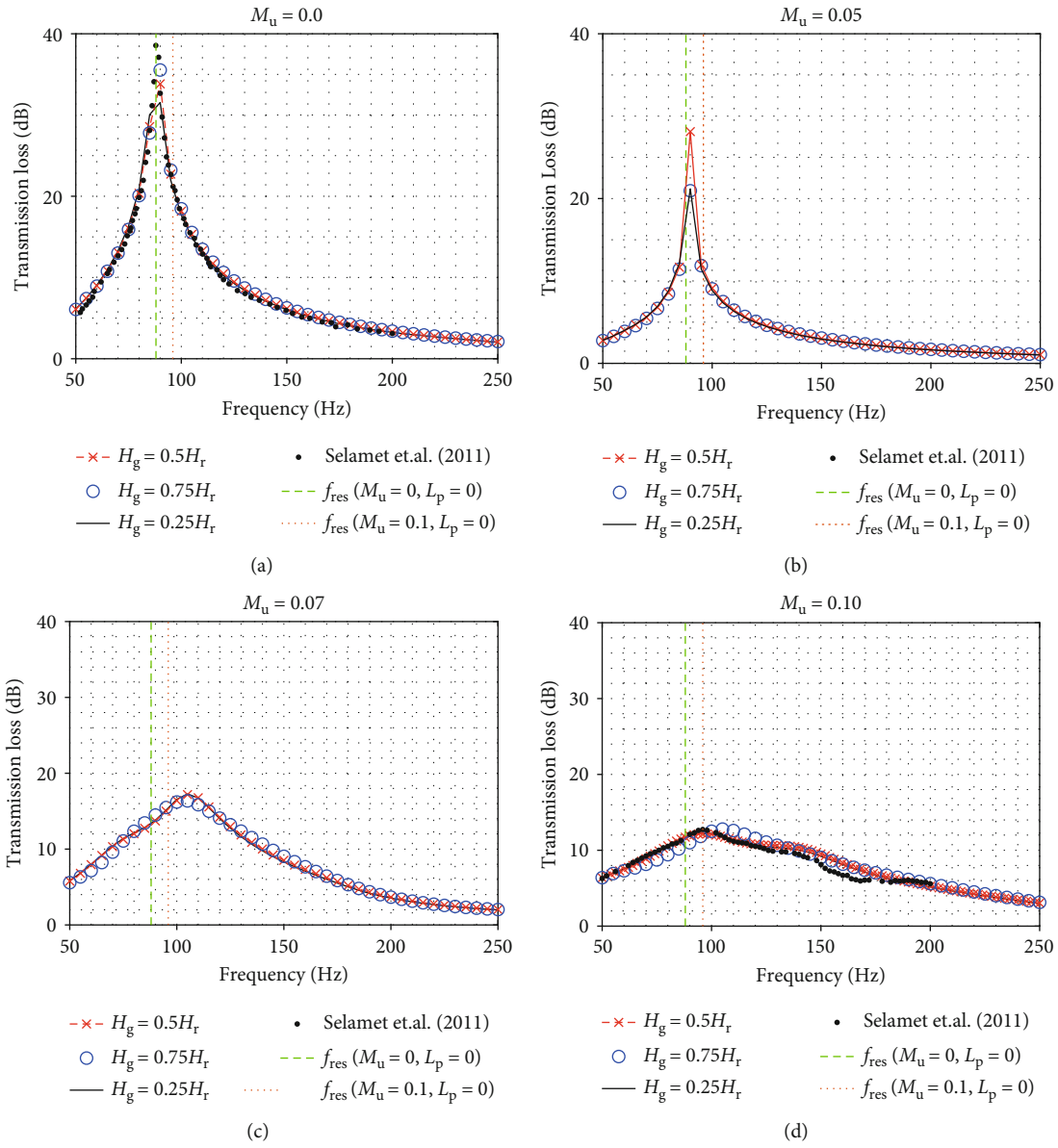

Figure 5: Variation of the transmission loss with forcing frequency, as $L_p = 0.5D_r$ and the rigid baffle is attached at 3 different locations, i.e., $H_g/H_r = 0.25$, $H_g/H_r = 0.5$, and $H_g/H_r = 0.75$. (a) $M_u = 0$, (b) $M_u = 0.05$, (c) $M_u = 0.07$, and (d) $M_u = 0.10$.

numerical, 3D simulation and the experimental results is obtained in general. As the grazing flow Mach number is increased, the maximum transmission loss is found to be reduced dramatically. The corresponding resonant frequency is found to be shifted from 88 Hz to about 100 Hz, as M_u is increased from 0 to 0.1. This investigation reveals that the developed numerical tool is applicable to evaluate the acoustic attenuation performances of a HR (Helmholtz resonator) [34, 35], as there is a grazing mean flow.

Implementing a rigid baffle with a fixed thickness is proposed to improve the aeroacoustic damping performance of the Helmholtz resonator [36, 37]. There are 2 implementation configurations:

(i) Config. 1: the rigid baffle is attached to the right sidewall of the resonator

(ii) Config. 2: the rigid baffle is attached to the left sidewall of the resonator

With the conventional design (i.e., $L_p/D_r = 0$), there are 3 different configurations. Figure 4 shows the comparison of the transmission loss with the same dimension rigid baffle implemented in these different configurations. It is revealed that for a given M_u (i.e., the grazing flow Mach number), transmission loss is generally independent on the implementation configuration. Further observation shows that implementing the rigid baffle with $H_g/H_r = 0.5$ and $L_p/D_r = 0.5$ does not improve the transmission loss performance in comparison with the conventional Helmholtz resonator. This reveals that further studies are needed to shed light on the dimensions and geometric implementing location of the rigid baffle. This is summarized and discussed in details later.

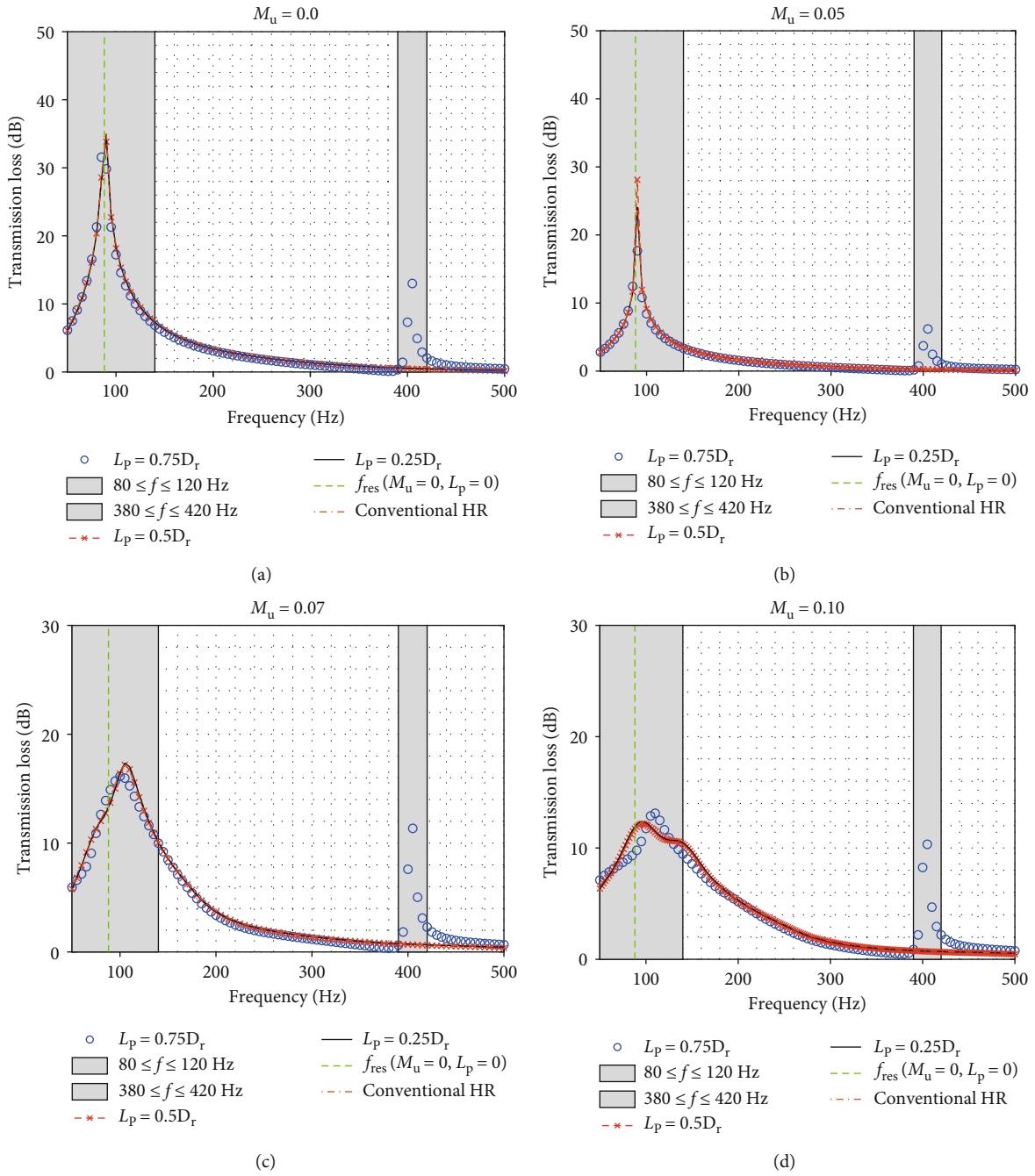

FIGURE 6: Variation of the transmission loss with forcing frequency, as the rigid baffle is attached at $H_g = 0.5H_r$ but 3 different widths, i.e., $L_p/D_r = 0.25$, $L_p/D_r = 0.5$, and $L_p/D_r = 0.75$. (a) $M_u = 0$, (b) $M_u = 0.05$, (c) $M_u = 0.07$, and (d) $M_u = 0.10$.

3. Results and Discussing Remarks

3.1. Effect of Implementing the Rigid Baffle. With the model being validated, the Helmholtz resonator with a rigid baffle attached to the right sidewall is numerically studied, as the grazing flow Mach number M_u is set to 4 different values. Figure 5 shows the transmission loss varied with forcing frequency for a given M_u, as $L_p/D_r = 0.5$ and the rigid baffle is attached at 3 different locations, i.e., $H_g/H_r = 0.25$, $H_g/H_r = 0.5$, and $H_g/H_r = 0.75$. It can be seen that varying H_g does not lead to a dramatic change of transmission loss, when M_u is set to 0, 0.07, and 0.1. However, the implementation of the rigid baffle leads to the dominant resonant frequency f_{res} being increased slightly at $M_u \ge 0.07$. However, the global maximum transmission loss is not altered. In addition, a closer observation shows that increasing M_u leads to the dominant f_{res} being increased dramatically, for a specified H_g. The global maximum transmission loss is found to decrease dramatically, as M_u is varied from 0 to 0.1.

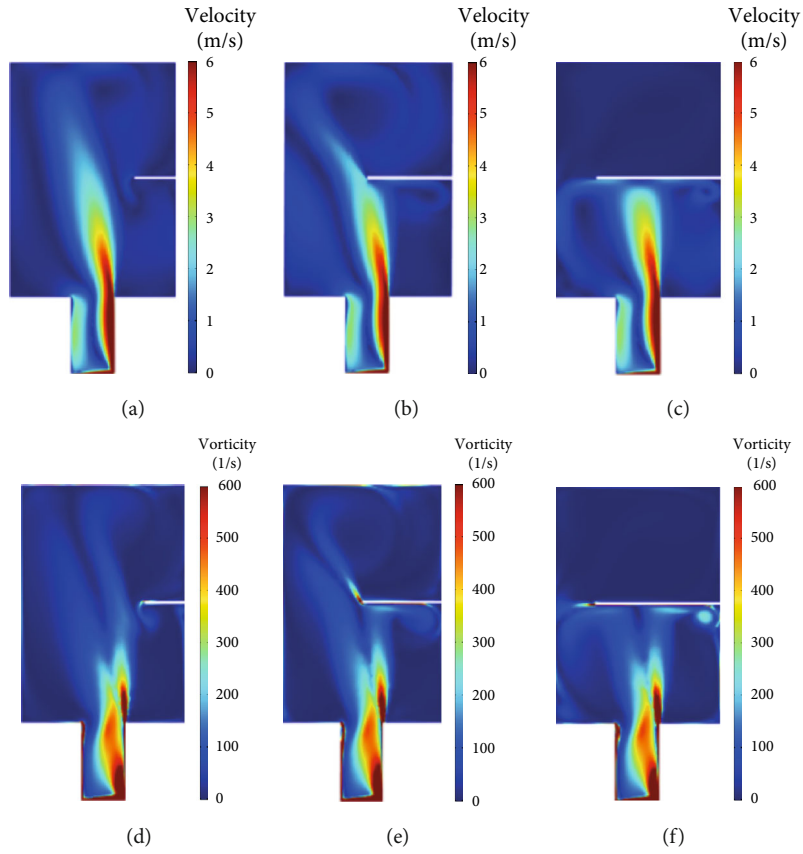

FIGURE 7: Comparison of the velocity and vorticity contours, as $M_u = 0.1$, the rigid baffle is attached at $H_g = 0.5H_r$ and L_p/D_r is changed from 0.25 to 0.5 and 0.75. (a, d) $L_p/D_r = 0.25$; (b, e) $L_p/D_r = 0.5$; (c, f) $L_p/D_r = 0.75$.

The effect of the rigid baffle length L_p on the transmission loss is evaluated and summarized in Figure 6. It shows the variation of the transmission loss with forcing frequency f for a given M_u, as the rigid baffle is attached at $H_g = 0.5H_r$ but 3 different widths, i.e., $L_p/D_r = 0.25$, $L_p/D_r = 0.5$, and $L_p/D_r = 0.75$. Comparison with the resonant frequency of the conventional Helmholtz resonator (i.e., $f_{res}(M_u = 0, L_p = 0)$) denoted by the green dash line is also made. It can be seen that there are two local peaks of transmission loss, as the length L_p/D_r of the rigid baffle is increased to 0.75. It reveals that implementing the rigid baffle with a length of $L_p/D_r = 0.75$ broadens the effective frequency range of the resonator by introducing one additional transmission loss peak at around 400 Hz. The corresponding secondary maximum transmission loss is approximately 12 dB. As M_u is increased from 0 to 0.10, the global maximum TL (transmission loss) is reduced significantly. In addition, a closer observation of Figures 6(c) and 6(d) shows that increasing L_p/D_r from 0.25 to 0.75 gives rise to the global maximum transmission loss being increased slightly. However, the dominant peak at around 100 Hz is more "flattened" at $L_p/D_r \leq 0.5$. This is especially true at $M_u = 0.1$ as shown in Figure 6(d).

In order to shed lights on the physics behind the 2 transmission loss peaks, vorticity contours and velocity contours are captured, as the rigid baffle is attached at $H_g/H_r = 0.5$ but with 3 different L_p. These are illustrated in Figure 7, as $M_u = 0.1$. It is apparent that as $L_p/D_r \leq 0.5$, a large clockwise vortex is locked in the resonator cavity, as shown in Figures 7(a), 7(b), 7(d), and 7(e). However, when $L_p/D_r = 0.75$, dual counterrotating vortexes are locked in the cavity below the rigid baffle, which is part of the original resonator's cavity. In other words, the rigid baffle acts like the "backplate" of the "smaller resonant cavity." In the cavity above the rigid baffle, there is no clear observation of any lock-in vortex, as shown in Figures 7(c) and 7(f). In general, the 2nd transmission loss peak is generated due to the structure modification, i.e., introducing the rigid baffle. The interaction between the modified structure and the incident sound leads to the generation of multiple resonance peaks in the transmission loss spectrum, as shown in Figure 6.

3.2. Effect of the Grazing Flow Mach Number. The grazing flow Mach number M_u effect on the aeroacoustic damping performance [3, 38–40] of the modified Helmholtz resonator is evaluated and discussed now. Figure 8 illustrates the modified resonator's damping behaviours over the interested frequency range, as the rigid baffle is attached at $H_g = 0.5H_r$, but its width L_p is set to 3 different values. It can be seen that when $L_p/D_r \leq 0.5$, there is only one TL (transmission loss) peak over the studied frequency range. However,

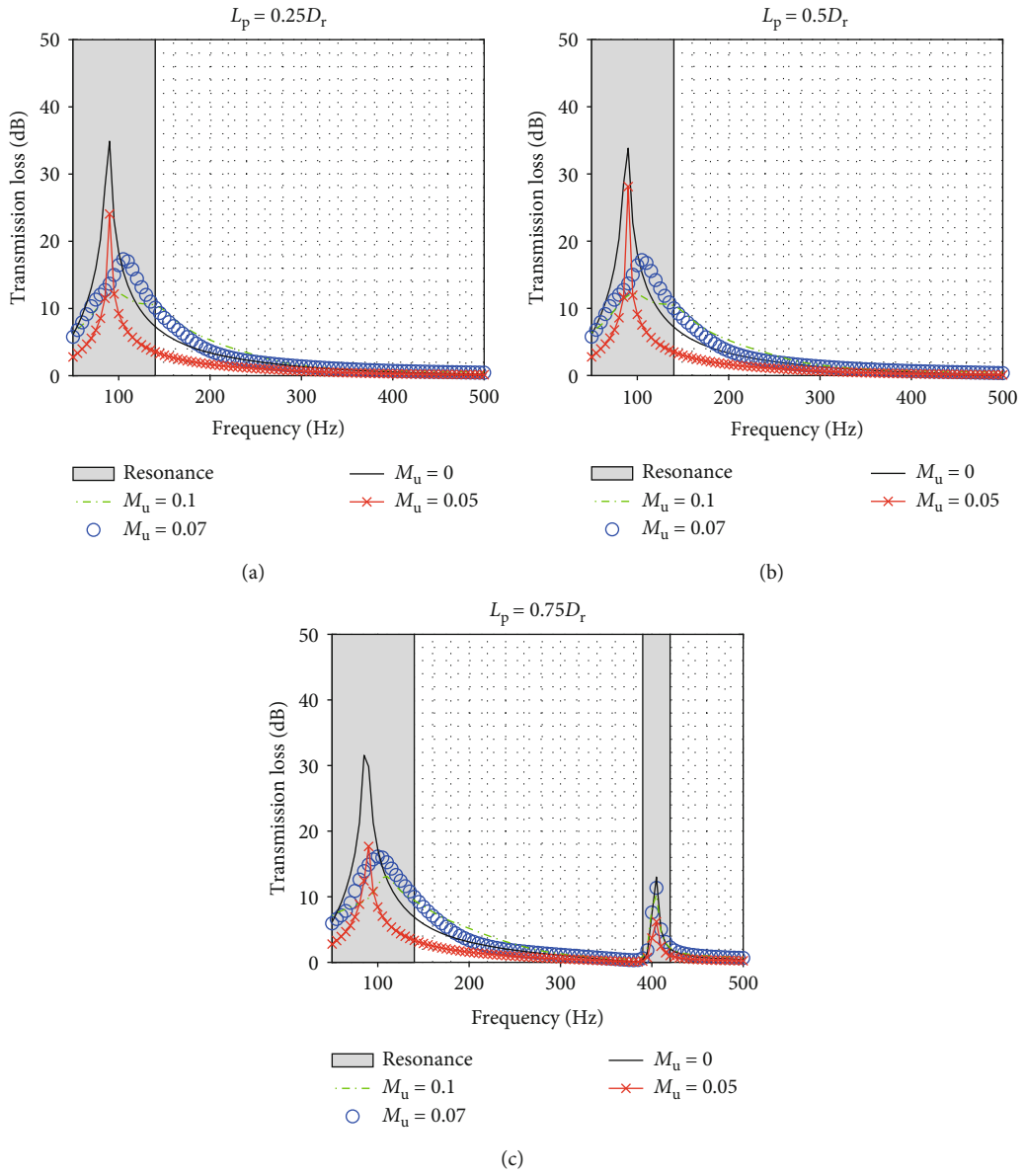

FIGURE 8: Transmission loss varied with the forcing frequency, as M_u is set to 4 different values and the rigid baffle is attached at $H_g/H_r = 0.5$ and L_p/D_r is changed from 0.25 to 0.5 and 0.75. (a) $L_p/D_r = 0.25$, (b) $L_p/D_r = 0.5$, and (c) $L_p/D_r = 0.75$. Upper cavity resonance frequency is 411 Hz corresponding to $L_{eff} = H_p + 0.612^*(0.25^*D_r)/4$. The original Helmholtz resonator in the absence of the baffle is 89 Hz.

one additional peak is observed, as $L_p/D_r = 0.75$. As M_u is increased from 0 to 0.1, the global TL_{max} is decreased for a given L_p. This means that the nonnegligible grazing flow deteriorates the acoustic damping effect of the modified structure Helmholtz resonator. In addition, one additional transmission loss peak is obtained at around 400 Hz, when $L_p/D_r = 0.75$. This additional peak in terms of the maximum value and the corresponding resonant frequency is independent on M_u.

Figure 9 summarizes the variation trend of the global maximum TL with the implementing location H_g and M_u, as the rigid baffle width is set to $L_p = 0.5D_r$. It illustrates that in the presence of a low Mach number grazing flow, i.e., $M_u \leq 0.05$, H_g does affect the acoustic attenuation performance of the modified Helmholtz resonator [33, 41]. However, as M_u is increased above 0.05, the attached location is found to play a negligible role on affecting the resonator's damping performance. This is most likely due to the fact that the vortex damping mechanism is based on the resonance of the entire resonator cavity [41, 42], since the grazing flow is nonnegligible ($M_u \geq 0.05$). This is clearly visualized in Figures 7(b) and 7(e). As $L_p/D_r = 0.5$, the rigid baffle does not contribute significantly to the acoustic damping performance in the presence of a larger Mach number grazing flow.

3.3. Effect of the Implementation Configurations. The rigid baffle could be implemented in 2 different configurations,

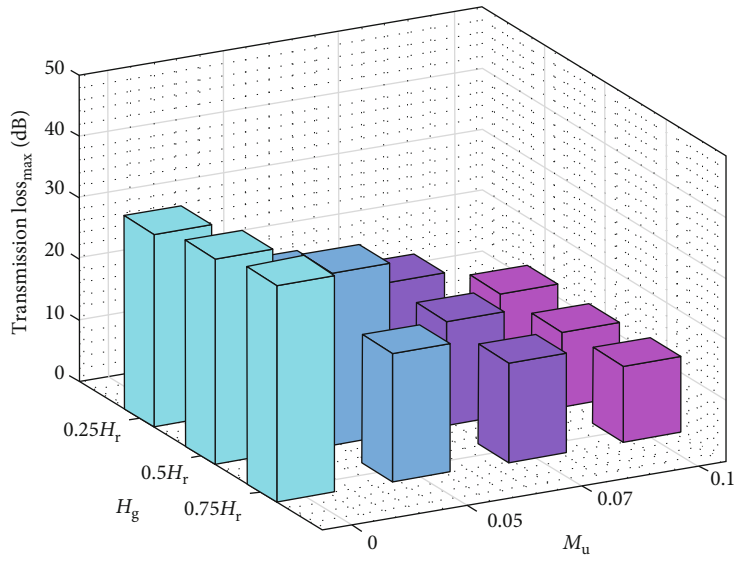

Figure 9: Variation of the global maximum transmission loss with the implementing height H_g and the grazing flow Mach number M_u, as the baffle width is set to $L_p/D_r = 0.5$.

i.e., attaching to the left or right sidewall of the resonator. These configurations are schematically shown in Figure 1 and described in Section 2.2. The effects of these implementation configurations are evaluated and compared, as M_u is set to 4 different values. Figure 10 illustrates the TL (transmission loss) performances of the modified Helmholtz resonator with frequency, as $H_g/H_r = 0.5$, $L_p/D_r = 0.75$, and the rigid baffle is implemented in 2 different configurations. It can be seen that the implementation configurations play a negligible role on affecting the transmission loss, especially when $M_u \leq 0.07$. When the grazing flow Mach number is increased to $M_u = 0.1$, the dominant resonant frequency corresponding to Config. 2 is approximately 10 Hz larger than that of the Config. 1. However, the secondary resonant frequency is almost unchanged, no matter to which sidewall the rigid baffle is attached. Furthermore, the difference of the local maximum transmission losses (corresponding to the 2 local peaks) between the 2 implementation configurations is less than 2.0 dB.

To shed lights on the dominant and the secondary resonant frequencies and the corresponding maximum transmission loss difference (see Figure 11(d)), the acoustic pressure contours of the Helmholtz resonator with the rigid baffle implemented are calculated. The acoustic pressure contours at the dominant resonant frequency are shown in Figures 12(a) and 12(b) as the rigid baffle is attached to the right and left sidewall, respectively, while the secondary resonant frequency contours are illustrated in Figures 12(c) and 12(d).

It can be seen that at the dominant resonant frequency, see Figures 12(a) and 12(b), vortex shedding is generated at the resonant neck. However, no vortex is observed in the cavity and the cavity is "resonant" as the baffle were not present. This is most likely due to the lower frequency and the longer wavelength. However, as the resonant frequency is increased to approximately 410 Hz as shown in Figures 12(c) and 12(d), the resonator is "resonant," like two connected [43–45] but separated cavities with a smaller volume due to the presence of the baffle. This could be the main physics behind the 1-2 dB improved transmission loss peak performance as shown in Figure 11(d) and the generation of the high-frequency transmission loss peak.

3.4. Effect of the Neck Shape of the Modified Helmholtz Resonator. Further design of the modified resonator is proposed by changing its neck shape. Here, we propose and test 1 additional shape, with the cross-sectional view of arc-shape "(·)," in addition to the conventional resonator neck shape, i.e., |·|. Figure 13 illustrates the computational unstructured mesh of the 2D-modelled Helmholtz resonator [28] with an arc-shaped neck and a rigid baffle implemented. The total number of cells is 960219.

Figure 10 shows the transmission loss performance of the arc-shaped Helmholtz resonator with a rigid baffle implemented. Its performances at different Mach numbers are evaluated and compared with those of the conventional |.|-shaped resonator. It can be seen that the resonant frequency in Hz corresponding to the dominant TL (transmission loss) peak is increased in general, as shown in Figures 10(a)–10(c). For example, 20% increase of the resonant frequency is observed at $M_u = 0.07$, as shown in Figure 10(c). In addition, the local maximum transmission loss at the secondary peak is increased by approximately 2-5 dB. This means that modifying the structure of the Helmholtz resonator, such as the neck shape, or implementing a rigid baffle leads to the shift of the resonant frequency and the improvement on the secondary transmission loss peaks. The improvement is most likely due to the increased equivalent cross-sectional area of the resonator neck with the arc shape. These are beneficial in the design of an effective Helmholtz resonator with a broader frequency range and a larger acoustic damping effect [46, 47].

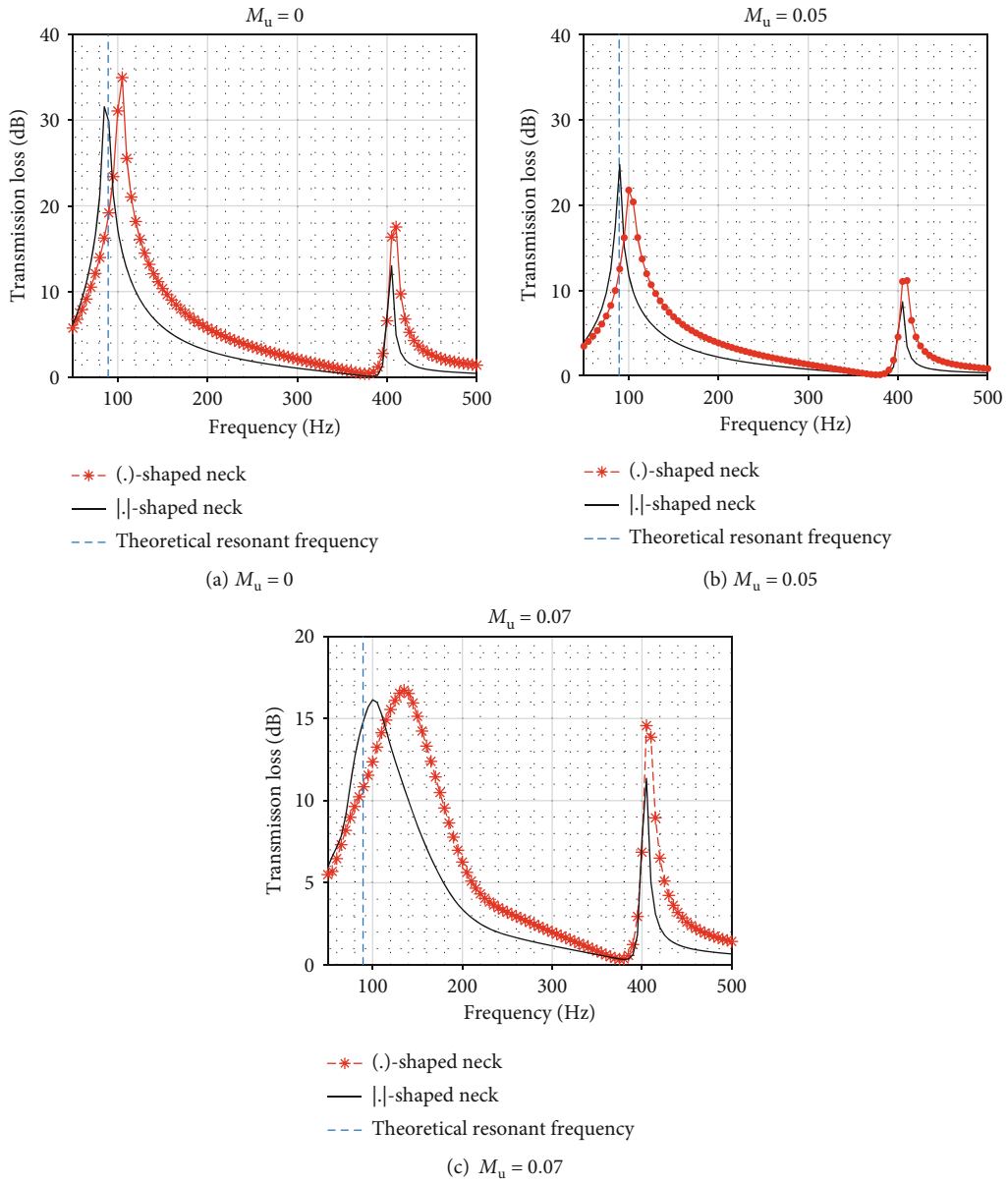

Figure 10: Comparison of the transmission loss performances, as the resonator neck shape is changed from the conventional |·| to arc (·) configuration. Here, the rigid baffle dimensions are set to be $L_p/D_r = 0.75$, $H_g/H_r = 0.5$.

4. Conclusions

Experimental and 2D numerical investigations are conducted on a cold-flow duct with a Helmholtz resonator (HR) implemented. A mean flow is forced to pass tangentially over the HR. It is also known as a grazing flow. The Mach number of the grazing flow is variable ($0 \le M_u \le 0.1$). Unlike the conventional one, the modified resonator is involved with an attached rigid baffle. Here, the rigid baffle could be attached in 2 different configurations, i.e., attaching to the left sidewall or right sidewall with reference to the duct flow direction. Five main variables are evaluated. These identified variables include (1) the width of the rigid baffle L_p, (2) the implementation location/height of the baffle H_g, (3) the grazing flow Mach number M_u, (4) the implementation configurations, and (5) the neck shape. Before applying the model to predict the transmission loss performances of the modified resonators, it is benchmarked first with the available experimental and 3D numerical data. Good agreement is achieved, as M_u is varied from 0 to 0.1. The model is then used to evaluate the acoustic attenuating performance of the modified resonator with the rigid baffle attached, as a nonnegligible duct flow is present. The key findings obtained from the current investigation are summarized as follows:

(i) When the grazing flow Mach number is small ($M_u \le 0.05$), the implementation location of the rigid baffle is found to affect the transmission loss of the modified Helmholtz resonator

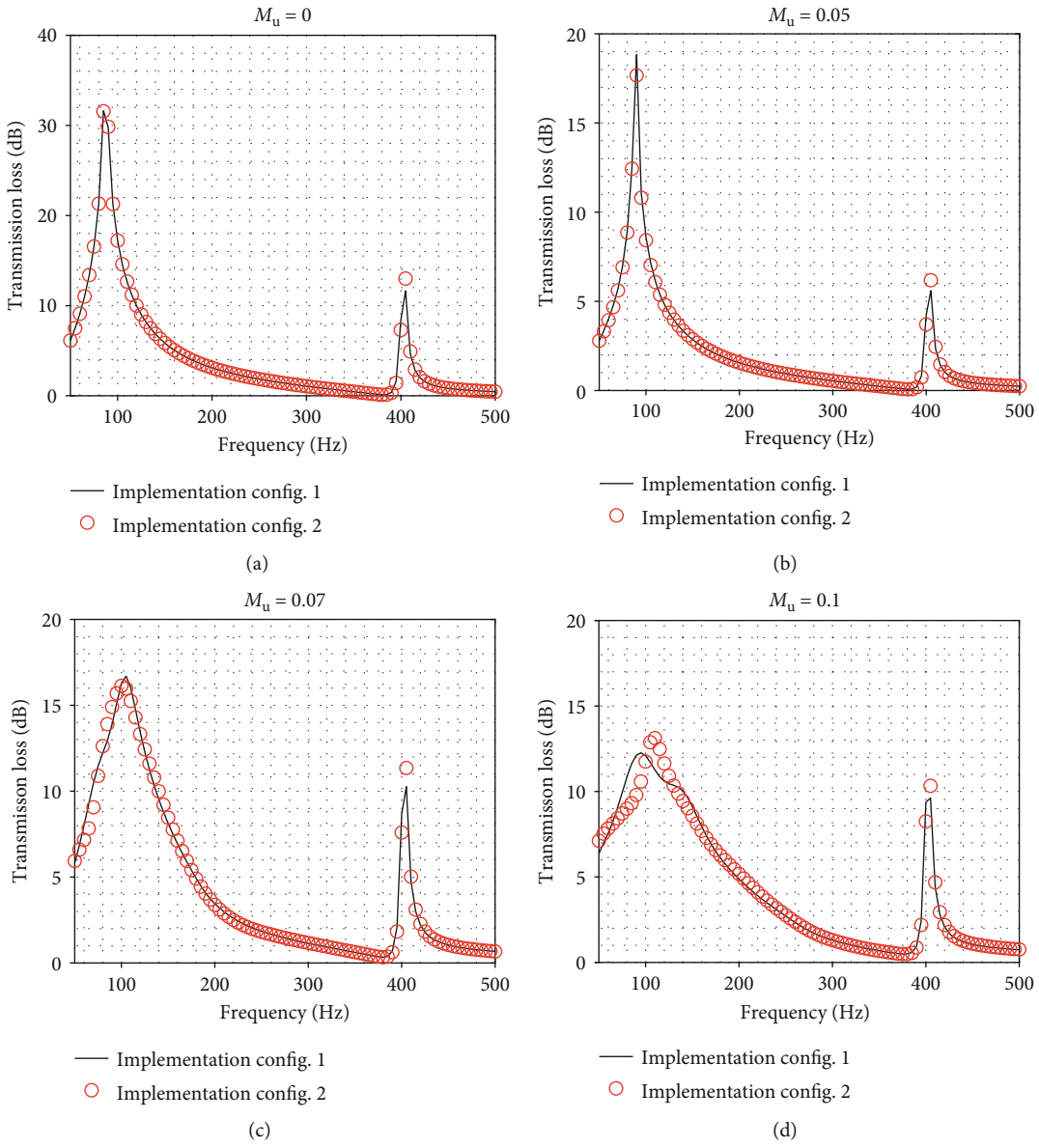

FIGURE 11: Comparison of the transmission loss performances of the modified Helmholtz resonator, as $H_g = 0.5H_r$, $L_p = 0.75D_r$, and the rigid baffle is implemented in 2 different configurations. (a) $M_u = 0$, (b) $M_u = 0.05$, (c) $M_u = 0.07$, and (d) $M_u = 0.1$.

(ii) In the presence of a nonnegligible grazing flow or the rigid baffle, the theoretical formula $\omega^2 = \pi c^2 D_n{}^2/4V_r L_{eff}$ fails in determining the resonant frequency of the modified Helmholtz resonator

(iii) As the duct flow Mach number is higher than 0.07 and $L_p/D_r \leq 0.5$, the implementation location of the rigid baffle is found to play a negligible role on affecting the transmission loss of the modified Helmholtz resonator

(iv) Increasing the Mach number of the duct flow leads to a deteriorated acoustic attenuation effect of the modified resonator in general

(v) When the width of the rigid baffle is increased to $L_p = 0.75D_r$, two transmission loss peaks at two different frequencies are observed. This is most likely due to the incident sound and structure interaction. The grazing flow Mach number is shown to affect strongly the dominant transmission loss peak

(vi) The secondary transmission loss peak at a higher frequency is found to be unchanged, as the grazing flow is varied. The flow characteristic contours reveal that the higher frequency peak is generated due to the "dual" vortex that is locked in the smaller cavity built by the rigid baffle and the neck

(vii) As the width of the rigid baffle is less than $0.5D_r$, there is an optimum grazing flow Mach number, which gives rise to a larger global maximum transmission loss

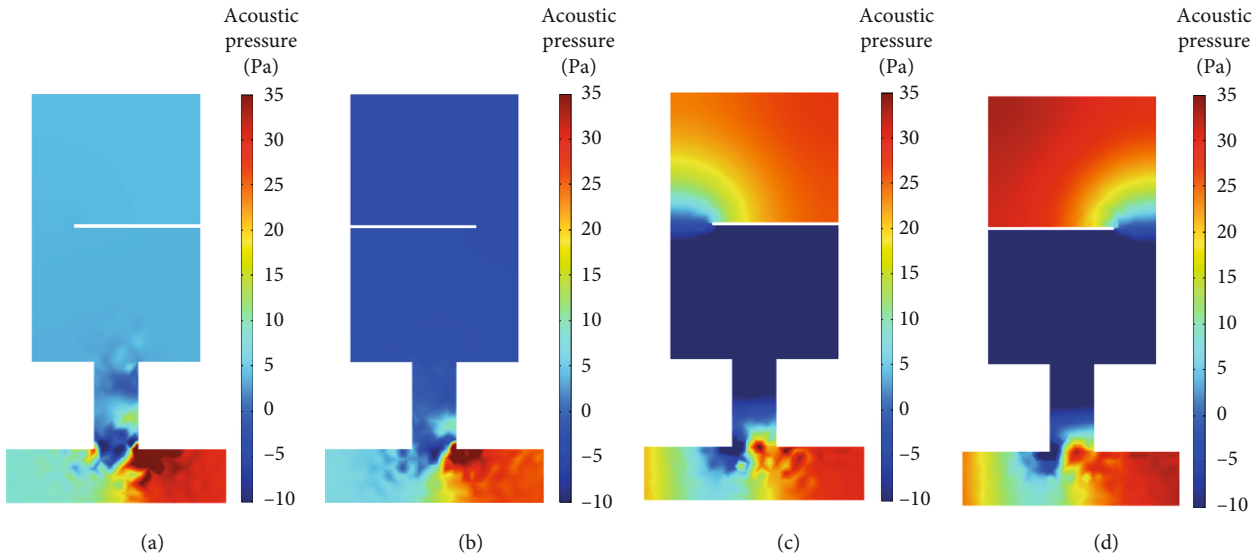

Figure 12: Comparison of the calculated contours of acoustic pressure at the dominant resonant frequency (a, b) and the secondary resonant frequency (c, d), as the rigid baffle is either attached to (a–c) right sidewall or (b, d) left sidewall. Here, $M_u = 0.1$ and $H_g/H_r = 0.5$ and $L_p = 0.75D_r$.

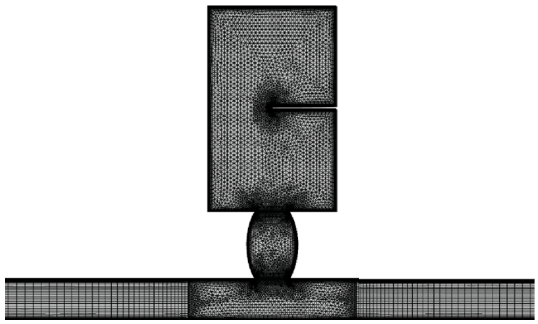

Figure 13: Mesh of the Helmholtz resonator with an arc-shaped neck and a rigid baffle implemented.

(viii) Changing the neck shape from the conventional $|\cdot|$ to an arc $(\cdot)$ one results in the dominant resonant frequency being increased by approximately 20%. The secondary transmission loss peak is increased by 2-5 dB. This is due to the increased equivalent neck cross-sectional area of the arc-shaped resonator

In general, the present work systematically studies an improved design of a Helmholtz resonator with an additional transmission loss peak at a high frequency, besides the dominant peak at a low frequency. How to improve the transmission loss peak at the high frequency is proposed. It is found that 5-10 dB more transmission loss could be achieved by changing the resonator neck shape from the conventional shape of $|\cdot|$ into the angle-bracket-"$(\cdot)$" one.

Data Availability

Data will be available on reasonable request.

Conflicts of Interest

The authors declare that there is no conflict of interest.

Acknowledgments

This work is financially supported by the Singapore National Research Foundation (Prime Minister Office), NRF2016NRF-NSFC001-102, and the University of Canterbury, New Zealand, with grant No. 452STUPDZ. This financial support is gratefully acknowledged.

References

[1] E. Selamet, A. Selamet, A. Iqbal, and H. Kim, "Effect of flow on Helmholtz resonator acoustics: a three-dimensional computational study vs. experiments," in *SAE Technical Paper Series*, Grand Rapids, Michigan, USA, May 2011.

[2] D. L. Gysling, G. S. Copeland, D. C. McCormick, and W. M. Proscia, "Combustion system damping augmentation with Helmholtz resonators," *Journal of Engineering for Gas Turbines and Power*, vol. 122, no. 2, pp. 269–274, 2000.

[3] I. D. J. Dupeŕe and A. P. Dowling, "The use of Helmholtz resonators in a practical combustor," *Journal of Engineering for Gas Turbines and Power*, vol. 127, no. 2, pp. 268–275, 2005.

[4] C. H. Sohn and J. H. Park, "A comparative study on acoustic damping induced by half-wave, quarter-wave, and Helmholtz resonators," *Aerospace Science and Technology*, vol. 15, no. 8, pp. 606–614, 2011.

[5] F. J. Fahy and C. Schofield, "A note on the interaction between a Helmholtz resonator and an acoustic mode of an enclosure," *Journal of Sound and Vibration*, vol. 72, no. 3, pp. 365–378, 1980.

[6] R. C. Chanaud, "Effects of geometry on the resonance frequency of Helmholtz resonators," *Journal of Sound and Vibration*, vol. 178, no. 3, pp. 337–348, 1994.

[7] F. Langfeldt, H. Hoppen, and W. Gleine, "Resonance frequencies and sound absorption of Helmholtz resonators with multiple necks," *Applied Acoustics*, vol. 145, pp. 314–319, 2019.

[8] A. Selamet, N. S. Dicky, and J. M. Novak, "Theoretical, computational and experimental investigation of Helmholtz resonators with fixed volume: lumped versus distributed analysis," *Journal of Sound and Vibration*, vol. 187, no. 2, pp. 358–367, 1995.

[9] R. C. Chanaud, "Effects of geometry on the resonance frequency of Helmholtz resonators, part II," *Journal of Sound and Vibration*, vol. 204, no. 5, pp. 829–834, 1997.

[10] J. F. Mercier, J. J. Marigo, and A. Maurel, "Influence of the neck shape for Helmholtz resonators," *The Journal of the Acoustical Society of America*, vol. 142, no. 6, pp. 3703–3714, 2017.

[11] A. S. Hersh, B. E. Walker, and J. W. Celano, "Helmholtz resonator impedance model, part 1: nonlinear behavior," *AIAA Journal*, vol. 41, no. 5, pp. 795–808, 2003.

[12] K. Förner and W. Polifke, "Nonlinear aeroacoustic characterization of Helmholtz resonators with a local-linear neuro-fuzzy network model," *Journal of Sound and Vibration*, vol. 407, pp. 170–190, 2017.

[13] A. Selamet and I. Lee, "Helmholtz resonator with extended neck," *The Journal of the Acoustical Society of America*, vol. 113, no. 4, pp. 1975–1985, 2003.

[14] A. Selamet, M. B. Xu, I. J. Lee, and N. T. Huff, "Helmholtz resonator lined with absorbing material," *The Journal of the Acoustical Society of America*, vol. 117, no. 2, pp. 725–733, 2005.

[15] P. K. Tang and W. A. Sirignano, "Theory of a generalized Helmholtz resonator," *Journal of Sound and Vibration*, vol. 26, no. 2, pp. 247–262, 1973.

[16] D. Li and L. Cheng, "Acoustically coupled model of an enclosure and a Helmholtz resonator array," *Journal of Sound and Vibration*, vol. 305, no. 1-2, pp. 272–288, 2007.

[17] S. Griffin, S. A. Lane, and S. Huybrechts, "Coupled Helmholtz resonators for acoustic attenuation," *Journal of Vibration and Acoustics*, vol. 123, no. 1, pp. 11–17, 2001.

[18] T. A. Johansson and M. Kleiner, "Theory and experiments on the coupling of two Helmholtz resonators," *The Journal of the Acoustical Society of America*, vol. 110, no. 3, pp. 1315–1328, 2001.

[19] M. B. Xu, A. Selamet, and H. Kim, "Dual Helmholtz resonator," *Applied Acoustics*, vol. 71, no. 9, pp. 822–829, 2010.

[20] C. Cai and C. M. Mak, "Hybrid noise control in a duct using a periodic dual Helmholtz resonator array," *Applied Acoustics*, vol. 134, pp. 119–124, 2018.

[21] W. V. Slaton and A. Nishikawa, "Aeroacoustic response of coaxial wall-mounted Helmholtz resonators in a low-speed wind tunnel," *The Journal of the Acoustical Society of America*, vol. 137, no. 1, pp. 253–260, 2015.

[22] S. S. Nudehi, G. S. Duncan, and U. Farooq, "Modeling and experimental investigation of a Helmholtz resonator with a flexible plate," *Journal of Vibration and Acoustics*, vol. 135, no. 4, article 041102, 2013.

[23] D. Zhao, "Transmission loss analysis of a parallel-coupled Helmholtz resonator network," *AIAA Journal*, vol. 50, no. 6, pp. 1339–1346, 2012.

[24] Z. Zhang, D. Zhao, N. Han, S. Wang, and J. Li, "Control of combustion instability with a tunable Helmholtz resonator," *Aerospace Science and Technology*, vol. 41, pp. 55–62, 2015.

[25] B. Ćosić, D. Wassmer, S. Terhaar, and C. O. Paschereit, "Acoustic response of Helmholtz dampers in the presence of hot grazing flow," *Journal of Sound and Vibration*, vol. 335, pp. 1–8, 2015.

[26] A. Selamet, P. M. Radavich, N. S. Dickey, and J. M. Novak, "Circular concentric Helmholtz resonators," *The Journal of the Acoustical Society of America*, vol. 101, no. 1, pp. 41–51, 1997.

[27] A. Selamet and Z. L. Ji, "Circular asymmetric Helmholtz resonators," *The Journal of the Acoustical Society of America*, vol. 107, no. 5, pp. 2360–2369, 2000.

[28] A. Selamet, M. B. Xu, I. J. Lee, and N. T. Huff, "A two-dimensional computational study of the flow effect on the acoustic behaviors of Helmholtz resonators," *International Journal of Vehicle Noise and Vibration*, vol. 6, no. 2, pp. 130–148, 2010.

[29] D. Yang, X. Wang, and M. Zhu, "The impact of the neck material on the sound absorption performance of Helmholtz resonators," *Journal of Sound and Vibration*, vol. 333, no. 25, pp. 6843–6857, 2014.

[30] Q. Mao, S. Li, and W. Liu, "Development of a sweeping Helmholtz resonator for noise control," *Applied Acoustics*, vol. 141, pp. 348–354, 2018.

[31] C. Cai and C. M. Mak, "Acoustic performance of different Helmholtz resonator array configurations," *Applied Acoustics*, vol. 130, pp. 204–209, 2018.

[32] X. L. Gai, T. Xing, X. H. Li, B. Zhang, and W. J. Wang, "Sound absorption of microperforated panel mounted with Helmholtz resonators," *Applied Acoustics*, vol. 114, pp. 260–265, 2016.

[33] J. Klaus, I. Bork, M. Graf, and G. P. Ostermeyer, "On the adjustment of Helmholtz resonators," *Applied Acoustics*, vol. 77, pp. 37–41, 2014.

[34] X. D. Zhao, Y. J. Yu, and Y. J. Wu, "Improving low-frequency sound absorption of micro-perforated panel absorbers by using mechanical impedance plate combined with Helmholtz resonators," *Applied Acoustics*, vol. 114, pp. 92–98, 2016.

[35] D. Zhao, C. Ji, J. Li, and L. Ang, "Experimental comparison of noise dissipation effects of single-and double-layer acoustic liners," *Applied Acoustics*, vol. 141, pp. 281–292, 2018.

[36] D. Zhao, Y. Sun, S. Ni, C. Ji, and D. Sun, "Experimental and theoretical studies of aeroacoustics damping performance of a bias-flow perforated orifice," *Applied Acoustics*, vol. 145, pp. 328–338, 2019.

[37] Z. B. Wang and Y. S. Choy, "Tunable parallel barriers using Helmholtz resonator," *Journal of Sound and Vibration*, vol. 443, pp. 109–123, 2019.

[38] A. Doria, "A simple method for the analysis of deep cavity and long neck acoustic resonators," *Journal of Sound and Vibration*, vol. 232, no. 4, pp. 823–833, 2000.

[39] G. Wu, Z. Lu, X. Xu et al., "Numerical investigation of aeroacoustics damping performance of a Helmholtz resonator: effects of geometry, grazing and bias flow," *Aerospace Science and Technology*, vol. 86, pp. 191–203, 2019.

[40] A. Sanada and N. Tanaka, "Extension of the frequency range of resonant sound absorbers using two-degree-of-freedom Helmholtz-based resonators with a flexible panel," *Applied Acoustics*, vol. 74, no. 4, pp. 509–516, 2013.

[41] R. Cora, C. A. Martins, and P. T. Lacava, "Acoustic instabilities control using Helmholtz resonators," *Applied Acoustics*, vol. 77, pp. 1–10, 2014.

[42] Z. Hu, C. Yang, and L. Cheng, "Acoustic resonator tuning strategies for the narrowband noise control in an enclosure," *Applied Acoustics*, vol. 134, pp. 88–96, 2018.

[43] D. Wu, N. Zhang, C. M. Mak, and C. Cai, "Hybrid noise control using multiple Helmholtz resonator arrays," *Applied Acoustics*, vol. 143, pp. 31–37, 2019.

[44] S. K. Tang, C. H. Ng, and E. Y. L. Lam, "Experimental investigation of the sound absorption performance of compartmented Helmholtz resonators," *Applied Acoustics*, vol. 73, no. 9, pp. 969–976, 2012.

[45] S. H. Seo, Y. H. Kim, and K. J. Kim, "Design of silencer using resonator arrays with high sound pressure and grazing flow," *Applied Acoustics*, vol. 138, pp. 188–198, 2018.

[46] G. Wu, S. Li, H. Zhao, X. Yang, and J. E, "Experimental and frequency-domain study of acoustic damping of single-layer perforated plates," *Aerospace Science and Technology*, vol. 69, pp. 432–438, 2017.

[47] A. Kierkegaard, S. Boij, and G. Efraimsson, "A frequency domain linearized Navier-Stokes equations approach to acoustic propagation in flow ducts with sharp edges," *The Journal of the Acoustical Society of America*, vol. 127, no. 2, pp. 710–719, 2010.